University of Groningen

Titanium Phosphate Grafted on Mesoporous SBA-15 Silica as a Solid Acid Catalyst for the Synthesis of 5-Hydroxymethylfurfural from Glucose

Guo, Wenze; Hensen, Emiel J. M.; Qi, Wei; Heeres, Hero; Yue, Jun

IMPORTANT NOTE: You are advised to consult the publisher's version (publisher's PDF) if you wish to cite from it. Please check the document version below.

Document Version
Publisher's PDF, also known as Version of record

Publication date:
2022

[Link to publication in University of Groningen/UMCG research database](#)

Citation for published version (APA):
Guo, W., Hensen, E. J. M., Qi, W., Heeres, H., & Yue, J. (2022). Titanium Phosphate Grafted on Mesoporous SBA-15 Silica as a Solid Acid Catalyst for the Synthesis of 5-Hydroxymethylfurfural from Glucose. *ACS Sustainable Chemistry & Engineering*, *10*(31), 10157–10168. https://doi.org/10.1021/acssuschemeng.2c01394, https://doi.org/10.1021/acssuschemeng.2c01394

Titanium Phosphate Grafted on Mesoporous SBA-15 Silica as a Solid Acid Catalyst for the Synthesis of 5-Hydroxymethylfurfural from Glucose

Wenze Guo, Emiel J. M. Hensen, Wei Qi, Hero J. Heeres, and Jun Yue*

ACCESS | Metrics & More | Article Recommendations | SI Supporting Information

ABSTRACT: The grafting of titania on SBA-15 followed by its phosphation was presented to prepare a mesoporous Lewis−Brønsted bifunctional solid acid catalyst for the tandem conversion of glucose via fructose to 5-hydroxymethylfurfural (HMF). Titania was dispersed on SBA-15 as an amorphous surface layer containing abundant coordinatively unsaturated tetrahedral Ti ions, which was reactive and readily transformed upon phosphation into a new titanium phosphate phase with the chemical formula identified as $Ti_2O_3(H_2PO_4)_2 \cdot 2H_2O$. The ordered mesoporous structure was well maintained after three modification cycles, affording a desirable surface area of over 300 m^2/g. The SBA-15-supported titanium phosphate layer affords higher overall acidity and Brønsted to Lewis acid ratio, compared with the conventional post-phosphated bulk anatase titania. The tetrahedral Ti ions and the adjacent protonated phosphate groups on the titanium phosphate layer could form Lewis−Brønsted acid pairs at molecular level proximity, which largely enhanced the selective tandem catalysis for glucose conversion via fructose to HMF. An optimized HMF yield of 71% was achieved at 160 °C in a water−methyltetrahydrofuran biphasic system over the SBA-15-supported titanium phosphate catalyst. The catalyst exhibited good hydrothermal stability with a rather limited silicon and phosphate leaching, and no distinct pore collapse or performance loss over three sequential reaction runs.

KEYWORDS: 5-hydroxymethylfurfural, glucose, titanium phosphate, SBA-15, solid acid
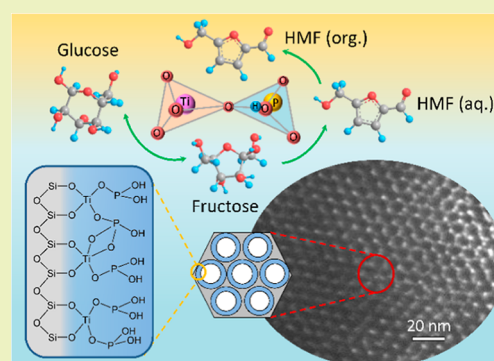
INTRODUCTION

The ever increasing living standards and global demand for energy and chemicals have led to a steady depletion of fossil resources and substantial environmental concerns related to CO_2 emissions. Significant research efforts have been directed toward utilizing lignocellulosic biomass as a green and sustainable alternative feedstock for the chemical industry.[1,2] In the envisioned biorefineries, 5-hydroxylmethylfurfural (HMF) is a typical furanic platform chemical, which can act as a bridge between carbohydrates and diverse value-added fuels, chemicals, and materials that are currently derived from traditional fossil resources.[3]

HMF is typically synthesized by the dehydration of C6 sugars such as fructose and glucose, with fructose being preferred in terms of the overall conversion rate and HMF selectivity.[4,5] However, glucose is a more attractive feedstock due to its lower price and higher abundance in nature compared with fructose and fructose-rich sources (high-corn fructose syrup, inulin, etc.).[6] In this context, significant research attention has been given to tandem catalysis comprising glucose isomerization to fructose over Lewis acid catalysts followed by fructose dehydration to HMF over Brønsted acid catalysts. Homogeneous Lewis acid catalysts (e.g., Al^{3+}-, Cr^{3+}-, and Zn^{2+}-based salts), combined with

mineral Brønsted acids such as HCl, H_2SO_4, and H_3PO_4, have been shown to be effective for the one-pot synthesis of HMF from glucose in water.[6−8] Nevertheless, heterogeneous catalysts are usually preferred over homogeneous ones due to the ease of catalyst separation and reuse, as well as the lower environmental impact. Therefore, zeolites, ion exchange resins, acid-functionalized metal oxides, metal phosphates, modified carbon, and their combinations have been explored as potential bi-functional solid acid catalysts affording one-pot tandem catalysis for glucose conversion to HMF.[9−11] It has been revealed that the bi-functionality of the solid Lewis/Brønsted acid (or acid/base) catalysts for glucose conversion is related to the relative amount, strength, as well as the proximity of the Lewis acid sites (LAS) and Brønsted acid sites (BAS),[12−14] and thus a proper tuning of these properties is critical to enhance the HMF yield.
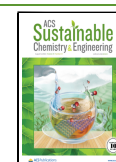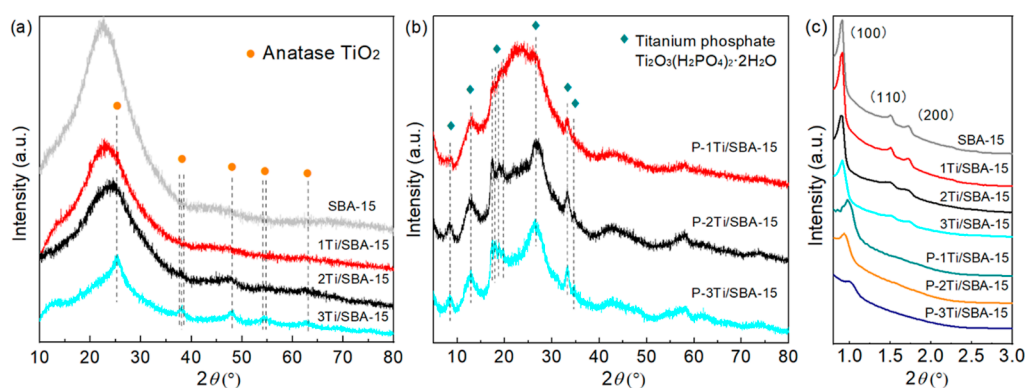
Figure 1. Wide-angle XRD patterns of (a) SBA-15 silica and titania grafted on SBA-15 and (b) phosphated titania (titanium phosphate) grafted on SBA-15 and (c) low-angle XRD patterns of SBA-15 and the grafted SBA-15 samples.

In a biorefinery, the sugar stream is mostly in the form of aqueous solution, which is produced from lignocellulose by fractionation methods such as steam explosion or enzymatic hydrolysis.[15] As such, using water as the reaction medium is preferred in terms of process simplification and energy conservation. Moreover, water as a green and cheap solvent is more economically and environmentally desirable compared with ionic liquids and polar aprotic organic solvents, despite side reactions occurring in water such as HMF rehydration to formic acid (FA) and levulinic acid, as well as the polymerization of sugars and HMF to humins. To suppress these side reactions, biphasic systems with the addition of a non-reactive organic phase to extract HMF formed in situ in the aqueous reaction phase has been developed and proven effective.[4−6,16−19] Other challenges that need to be addressed for reactions over solid acid catalysts in water include (i) the deactivation of LAS by hydration in water (e.g., zeolites);[20] (ii) the hydrolytic leaching of active functional groups (e.g., sulfate or phosphate groups on acid-functionalized metal oxides);[21] and (iii) the collapse of porous structures under hydrothermal reaction conditions.[22] Consequently, developing water-tolerant bi-functional solid acid catalysts for glucose conversion in water-organic biphasic systems is of great importance.

Transition-metal (Ti, Zr, or Hf) oxides have been reported to exhibit excellent activity in water and high availability for acid functionalization with anions such as sulfate, tungstate, and phosphate.[12,23−25] Recently, we reported a comprehensive approach on glucose conversion to HMF via the selective tandem catalysis over an in situ phosphated titania catalyst.[12] The phosphates were incorporated into the titania framework forming a titanium phosphate surface layer, where tetrahedral TiO_4 units (acting as water-tolerant LAS) and the adjacent protonated phosphates (behaving as BAS) could form Lewis−Brønsted acid pairs at molecular-level proximity. Such a close arrangement enhanced both glucose turnover and HMF selectivity, due to the rapid transfer of the formed fructose from LAS to BAS for its dehydration to HMF facilitating LAS liberation for another glucose turnover. Generally, these findings infer a promising catalytic property of metal phosphates for the tandem catalysis for glucose conversion, in line with the desirable HMF yields reported in the literature using phosphates of titanium, zirconium, tin, or hafnium as solid acid catalysts.[14,26−28] However, (post-phosphated) metal oxides and metal phosphates usually exhibit low surface areas and rather limited porosity in their native form,[14,28−30] which tend to restrict the amount and accessibility of the catalytic

acid sites on the inner surface for the chemical conversion of bulky biobased molecule and cause high pressure drop upon loading into continuous flow reactors as a packed bed.[12] Therefore, methods to synthesize and stabilize highly porous phosphated metal oxides or metal phosphates are required. The in situ phosphation method as presented in our previous work,[12] represents an effective way,[12] where titanium phosphate was created as a surface layer embedded onto the titania phase and inhibited the sintering of titania crystallite grains during the calcination, preventing the pore collapse and giving a desirable surface area of ca. 200−300 m^2/g.

Besides the direct synthesis, another possibility to improve the porosity could be found by dispersing titania or titanium phosphate onto a high-surface area scaffold with well-defined meso-porosity, for example, silica materials such as HMS-24, MCM-41, and SBA-15.[22] Zhang et al.[31] reported the grafting of titanium phosphate onto SBA-15 by (i) alternate grafting of $Ti(OPr^i)_4$ and then $POCl_3$ or (ii) one-pot reaction of $Ti(OPr^i)_4$ and $POCl_3$ in the presence of SBA-15. In both methods, the grafting procedures could be repeated in a layer-by-layer fashion to adjust the loading of titanium phosphate and thus, the pore size and acidity. Shintaku et al.[32] prepared TiO_4-deposited SBA-15 silica by a simple post-grafting method using $Ti(OPr^i)_4$. The catalyst maintained a large surface area (ca. 450 m^2/g) and ordered mesoporous structure, and the isolated TiO_4 tetrahedra therein afforded Lewis acidity even in the presence of water. Osatiashtiani et al.[22] synthesized ZrO_2-grafted SBA-15 which was then sulfated and used as solid acid catalyst for glucose conversion in water. It was found that the BAS/LAS ratio increased with the increasing layer thickness and sulfate loading, and the sulfated zirconia/SBA-15 delivered a 3-fold enhancement in HMF productivity over nonporous sulfated zirconia counterparts.

In this work, we present the grafting of titania on a high-surface area mesoporous SBA-15 silica, followed by a phosphation treatment to transform the titania layer into titanium phosphate as the solid acid catalyst for glucose conversion. The physiochemical properties of the dispersed titania or titanium phosphate were systematically characterized. The crystalline, textural, and compositional properties were studied using X-ray diffraction (XRD), N_2 sorption, Fourier transform infrared (FTIR), and thermal gravity analysis (TGA). The surface chemical states and acidic properties were revealed by X-ray spectroscopy (XPS), ammonia temperature-programmed desorption (NH_3-TPD), and infra-red spectroscopy of pyridine adsorption (Py-IR). The catalytic
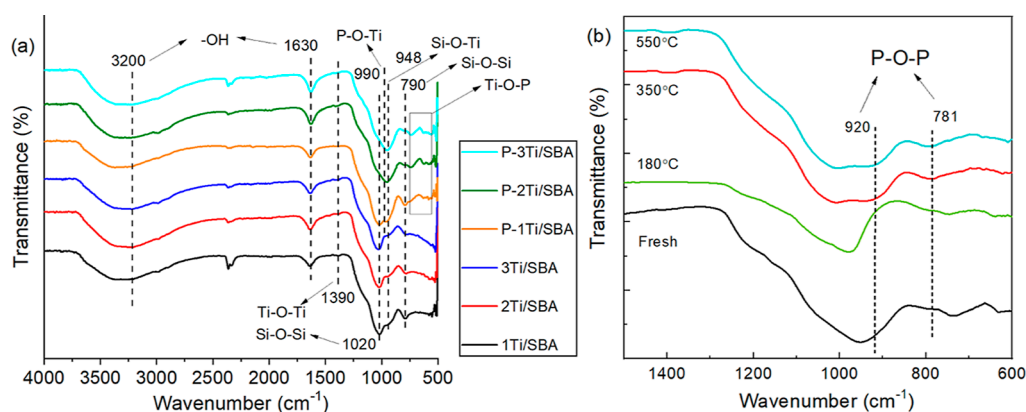
Figure 2. FTIR spectra of (a) titania and titanium phosphate layers on SBA-15 and (b) fresh P−3Ti/SBA-15 sample and those further calcined at 180, 350, or 550 °C for 6 h.

performance of the synthesized catalysts for glucose conversion to HMF was tested in a water-2-methyltetrahydrofuran (mTHF; a green biobased extraction solvent) biphasic solvent system. Finally, the hydrothermal stability and reusability of the catalysts were also evaluated.

RESULTS AND DISCUSSION

Titania was grafted onto the SBA-15 silica and subsequently phosphated to prepare titanium phosphate, as displayed in Scheme S1. Titania was first grafted via a surface sol−gel reaction between Ti(OPr^i)$_4$ and the surface hydroxyl groups (Si−OH) on SBA-15,[33] followed by a hydrolysis step to generate surface Ti−OH groups. This grafting cycle can be repeated to increase the titania loading (Scheme S1). The obtained materials were denoted as nTi/SBA-15, where n (= 1, 2 or 3) denotes the number of grafting cycles. The grafted titania layer was subsequently phosphated via a reaction with phosphoric acid, leading to phosphated titania (titanium phosphate) grafted on SBA-15, which was denoted as P-nTi/SBA-15. Additionally, bulk anatase titania was also prepared and phosphated via a conventional post-phosphation method. The resulting materials were used as the reference samples and denoted as TiO$_2$ and PO$_4$$^{3-}$/TiO$_2$, respectively. More details regarding the catalyst synthesis are given in the Experimental Section in the Supporting Information.

Crystalline, Textural Properties, and Composition Analysis. The crystalline structure of titania and the phosphated titania supported on SBA-15 silica was investigated by wide-angle XRD (Figure 1a,b). The pattern of pristine SBA-15 silica displays a broad peak at ca. $2\theta = 22°$, corresponding to a typical amorphous nature, which was still maintained after two grafting cycles (i.e., 1Ti/SBA-15 and 2Ti/SBA-15; Figure 1a). This indicates a relatively homogeneous coating of titania on SBA-15 without forming a 3-dimensional crystalline titania phase[22,31] until further increasing the grafting cycles up to three. Peaks corresponding to anatase titania started to emerge on the pattern of 3Ti/SBA-15, though in a weak intensity and relatively broad width (Figure 1a). After phosphation, the peaks of titania phase disappeared while a new crystalline phase showed up (Figure 1b). Such pattern and peak distribution (excluding that of SBA-15) are not recorded in the latest JCPDS database but are in good agreement with that from a novel titanium phosphate with a formula Ti$_2$O$_3$(H$_2$PO$_4$)$_2$· 2H$_2$O as reported in the literature.[34−36] In a control experiment, bulk anatase TiO$_2$ was phosphated under

otherwise the same conditions, while it turned out that the crystalline properties of the resulting PO$_4$$^{3-}$/TiO$_2$ remained nearly unchanged (Figure S1). Thus, the amorphous (or low crystallinity) titania grafted on SBA-15 is believed to be by far more reactive than bulk anatase titania toward phosphation and transformation into titanium phosphate. This is possibly due to a higher abundance of the coordinately unsaturated tetrahedra TiO$_4$ units present on the SBA-15-supported amorphous titania layer, which are less robust compared with bulk anatase with a high crystallinity structure (vide infra).[12,32]

The low-angle XRD patterns of SBA-15, nTi/SBA-15, and P-nTi/SBA-15 all display distinct peaks at 2θ of ca. 0.5°−2°, indicating a regular mesoporous structure, which was well maintained after the grafting of titania or titanium phosphate (Figure 1c). The peak intensity decreases with the increasing loading of titania or titanium phosphate (i.e., with more modification cycles), consistent with the gradual filling of mesopores and decrease of mesoporous orderliness.[31] The slight shift of peaks to higher angles with the increasing loading is also consistent with the decrease in d-spacing.[31]

IR spectroscopy was performed on the nTi/SBA-15 and P-nTi/SBA-15 samples to acquire their structural insights (Figure 2a). For all samples, the broad peaks at 3200 and 1630 cm^{-1} correspond to the hydroxyl groups and adsorbed water on the surface. The peaks at 1020 and 790 cm^{-1} are related to the Si−O−Si stretching and bending vibrations, respectively.[37] The interaction between SBA-15 silica and titania or titanium phosphate is shown in the Si−O−Ti bond at 948 cm^{-1}.[38] A weak peak is also present at 1390 cm^{-1} for all samples, which is attributed to Ti−O−Ti vibrations.[39] For P-nTi/SBA-15 samples, peaks corresponding to P−O stretching vibrations are present at ca. 990−1030 cm^{-1},[12] which tend to overlap with the neighboring peaks of, for example, Si−O−Si and Si−O−Ti, leading to a shift of the overall broad peak within the range of 948−1020 cm^{-1}. Moreover, peaks at 620−750 cm^{-1} are assigned to the Ti−O vibrations in the Ti−O−P matrix.[35,36]

TGA measurements were conducted for the compositional analysis of the newly formed titanium phosphate phase on SBA-15 (using P−3Ti/SBA-15 as an example; Figure 3). A total mass loss of ca. 19.5% was observed after heating from 25 to 700 °C, and the DTG curves revealed four main stages of mass loss. The first stage occurring before ca. 50 °C with a mass loss of ca. 4.5% is assigned to the desorption of physically adsorbed water. The following three stages led to mass losses
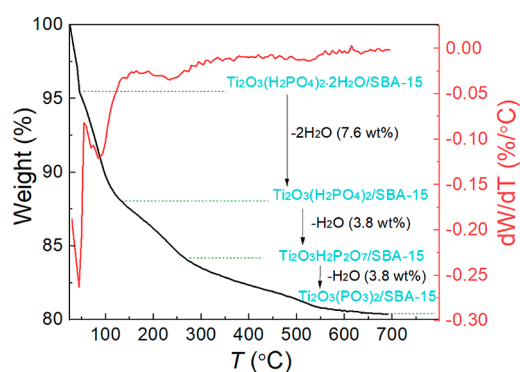
Figure 3. TGA and DTG curves of P−3Ti/SBA-15.

of 7.6%, 3.8%, and 3.8% for the temperature ranges of 50−150 °C, 150−300 °C, and 300−700 °C, respectively, which agree well with the formula $Ti_2O_3(H_2PO_4)_2 \cdot 2H_2O$ proposed by Bortun et al.[34] Concretely, the mass loss of the second stage is ascribed to the release of crystallization water [i.e., $Ti_2O_3(H_2PO_4)_2 \cdot 2H_2O/SBA-15 \rightarrow Ti_2O_3(H_2PO_4)_2/SBA-15$], and those of the third and fourth stages to the releases of the structurally bound water, which are accompanied by the condensation of the $-H_2PO_4$ groups of titanium phosphate into pyrophosphate and further into polyphosphate $[Ti_2O_3(H_2PO_4)_2/SBA-15 \rightarrow Ti_2O_3H_2P_2O_7/SBA-15 \rightarrow Ti_2O_3(PO_3)_2/SBA-15]$.

Furthermore, IR spectroscopy was measured for P−3Ti/SBA-15 samples that have been further calcined at different temperatures such as 180, 350, and 550 °C for 6 h to represent the different stages of thermal mass loss in TGA, as shown in Figure 2b. The fresh and 180 °C-heated P−3Ti/SBA-15 give similar spectra, corresponding to the second stage that only the crystalline water was released (Figure 3). After calcination at 350 and 550 °C, two new bands appeared at 920 and 781 cm^{-1} (corresponding to the asymmetric and symmetric P−O−P stretching vibrations, respectively) which are characteristic peaks of the condensed phosphates such as the pyrophosphate group $(P_2O_7^{4-})$.[34,36] As such, the FTIR spectra substantiate the pyrolytic process of titanium phosphate based on the TGA results (Figure 3). Generally, the above results of XRD, TGA,

and FTIR verified the formation of titanium phosphate $Ti_2O_3(H_2PO_4)_2 \cdot 2H_2O$ upon the phosphation of titania on SBA-15 silica.

The loading and composition of titania and titanium phosphate grafted on SBA-15 silica were confirmed by inductively coupled plasma-atomic emission spectroscopy (ICP-AES) analysis (Table 1). The content of Ti shows a logical increasing trend with increasing grafting cycles (n) for both nTi/SBA-15 and P-nTi/SBA-15 (entries 1−4 or 5−7). In principle, under the premise of a complete transformation of the grafted titania into titanium phosphate after phosphation, the P content of the resulting materials should be equally proportional to the corresponding Ti content, given the homogeneity of titanium phosphate. This has been reflected in the bulk composition of P-1Ti/SBA-15 and P-2Ti/SBA-15, giving P contents of 1.19 and 2.61 mmol/g, respectively, but with an identical bulk P/Ti molar ratio of 1.02 (entries 5, 6). Such a value corroborates the identified titanium phosphate phase with the chemical formula $[Ti_2O_3(H_2PO_4)_2 \cdot 2H_2O]$ indicating a P/Ti molar ratio of 1. Notably, P−3Ti/SBA-15 shows a reasonable surface P/Ti ratio of 1.03, but a lower P content than P−2Ti/SBA-15 and a smaller bulk P/Ti molar ratio of 0.59 (entry 7). This implies an incomplete conversion of titania on 3Ti/SBA-15, which could be due to that the higher titania loading (i.e., thicker titania layer) imposed more difficulties for H_3PO_4 to penetrate deeply from the surface into the titania framework. As a result, only a converted titanium phosphate outer layer could be generated atop an unconverted inner titania layer. Additionally, the presence of somewhat anatase titania crystalline with a robust nature on 3Ti/SBA-15 could have resisted the phosphation reaction (Figure 1a), leading to a less P content. Notably, such an incomplete phosphation and less bulk P content are not expected to have distinct effects on the catalytic activity of P−3Ti/SBA-15, as the reaction occurs only on the surface and should not be affected by the bulk composition of the catalyst. Generally, via grafting titania on SBA-15 followed by phosphation, the P loading and (both bulk and surface) P/Ti ratio of the prepared P-nTi/SBA-15 is at least one or two orders of magnitude higher than that of the conventional post-phosphated anatase titania (PO_4^{3-}/TiO_2), which should also lead to a significant

Table 1. Composition, Textural Structure, and Crystalline Properties of TiO_2, PO_4^{3-}/TiO_2, SBA-15, and the Grafted Catalysts[a]

| entry	catalyst	content[b] (mmol/g) P	content[b] (mmol/g) Ti	molar ratio P/Ti (−) bulk[b]	molar ratio P/Ti (−) surface[c]	S_{BET} (m²/g)	d_{BJH} (nm)	V_p (cm³/g)	a_0[d] (nm)	δ_{Wall}[e] (nm)	δ_{Layer}[f] (nm)
1	SBA-15	0	0			786	7.2	1.07	11.23	4.03	
2	1Ti/SBA-15	0	1.25	0		687	6.3	0.87	11.23	4.93	0.45
3	2Ti/SBA-15	0	3.32	0		600	5.3	0.70	11.23	5.93	0.95
4	3Ti/SBA-15	0	4.22	0		529	4.5	0.53	11.23	6.73	1.35
5	P−1Ti/SBA-15	1.19	1.17	1.02	n.d.[g]	594	5.9	0.82	11.12	5.22	0.60
6	P−2Ti/SBA-15	2.61	2.55	1.02	n.d.	474	4.8	0.66	11.02	6.22	1.09
7	P−3Ti/SBA-15	2.16	3.67	0.59	1.03	328	4.1	0.49	11.02	6.92	1.44
8	TiO_2	0	n.d.	0		36	3.6	0.80			
9	PO_4^{3-}/TiO_2	0.04	11.52	0.003	0.09	31	3.3	0.77			

[a]S_{BET}, d_{BJH}, and V_p in the table denote the BET specific surface area, BJH adsorption pore diameter, and pore volume, respectively. [b]Determined by ICP analysis. [c]Determined by XPS. [d]Hexagonal lattice parameter, calculated by $a_0 = 2d_{100}/\sqrt{3}$.[40] Here, d_{100} is the interplanar spacing of (100) plane and calculated by Bragg's equation $d_{100} = \lambda/2\sin\theta$, where λ is the X-ray wavelength (1.5418 Å) and θ the Bragg diffraction angle of (100) plane (cf. Figure 1c); [e]Average thickness of the pore wall, calculated by $\delta_{wall} = a_0 - d_{BJH}$.[40] [f]Average thickness of the grafted layer of titania or titanium phosphate, calculated by $\delta_{Layer} = (\delta_{wall} - \delta_{wall \, of \, SBA-15})/2$.[31] [g]not determined.

difference in the acid density and catalytic performance (vide infra).

The textural properties of nTi/SBA-15 and P-nTi/SBA-15 were characterized by N_2 physisorption (Figure S2 and Table 1). All samples exhibit a type IV isotherm, an H1 type hysteresis loop (Figure S2a), and a narrow pore size distribution (Figure S2b), corresponding to a uniform cylindrical mesoporosity and consistent with the low-angle XRD results (Figure 1c). A logical and regular decreasing trend was observed in the Brunauer−Emmett−Teller (BET) surface area, average pore size, and pore volume with the increasing grafting cycles (n) of titania and titanium phosphate, due to the gradual filling (rather than the local blocking) of the mesopores. The estimated average thickness of the pore wall and that of the grafted layer of titania or titanium phosphate increased accordingly, corresponding to their increased loading (Table 1; entries 1−7). A high surface area was maintained even after three grafting cycles, for example, 529 m^2/g for 3Ti/SBA-15 and 328 m^2/g for P−3Ti/SBA-15, which is significantly higher than that of the reference samples (i.e., only 36 m^2/g for bulk anatase TiO_2 and 31 m^2/g for PO_4^{3-}/TiO_2; see entries 8−9 of Table 1). Furthermore, the morphology of the catalysts was observed by transmission electron microscopy (TEM) (Figure 4). SBA-15 shows a typical well-ordered hexagonal mesoporous structure (Figure 4a,b). After the grafting of titania or titanium phosphate layers, the ordered mesopores were still maintained (Figure 4c−h), indicating a relatively homogeneous coating on SBA-15. Besides, a relatively rougher pore surface was observed for 3Ti/SBA-15 and P−3Ti/SBA-15 (Figure 4e,h), suggesting a slight decrease of the orderliness which is consistent with the low-angle XRD results (Figure 1c). The scanning TEM (STEM)−energy-dispersive X- ray (EDX) elemental mapping clearly shows a homogeneous distribution of Ti or P over the 3Ti/SBA-15 and P−3Ti/SBA-15 samples, which was also supported by the similar Ti and P content over the different spectra on the samples (cf. Figure 4i,j and the detailed quantification results in Figures S3, S4 in the Supporting Information). Generally, the results of N_2 physisorption, low-angle XRD, TEM, and STEM/EDX have revealed a relatively homogeneous deposition of titania or titanium phosphate on SBA-15 leading to a highly porous structure with a high surface area. This corroborates the advantages of the current synthesis method over the conventional post-phosphation method (which renders a non-porous PO_4^{3-}/TiO_2).

Surface Chemical State and Acid Properties. XPS characterizations were performed on 3Ti/SBA-15, P−3Ti/SBA-15, as well as TiO_2 and PO_4^{3-}/TiO_2 as the reference samples (Figure 5), to gain insights into the chemical state of the surface Ti ions that is strongly related to their acid properties and catalytic performance. For all samples, the Ti $2p_{3/2}$ region is fitted as two peaks at 459.3 and 458.8 eV (Figure 5a,b), indicating two different chemical states of the surface Ti ions. The peak at 458.8 eV corresponds to a saturated octahedral coordination with oxygen (TiO_6), while the other one at 459.3 eV belongs to Ti ions in a coordinately unsaturated tetrahedral environment (TiO_4).[12] Apparently, the majority of the surface Ti ions on the bulk anatase TiO_2 is in the octahedral coordination, whereas the tetrahedral Ti ions take up a larger portion on 3Ti/SBA-15 (Figure 5a). As a result, the overall Ti $2p_{3/2}$ peak for 3Ti/SBA-15 is at 459.3 eV, which is higher than that for TiO_2 (458.9 eV), with the atomic ratio of tetrahedral (459.3 eV) to octahedral (458.8 eV) Ti
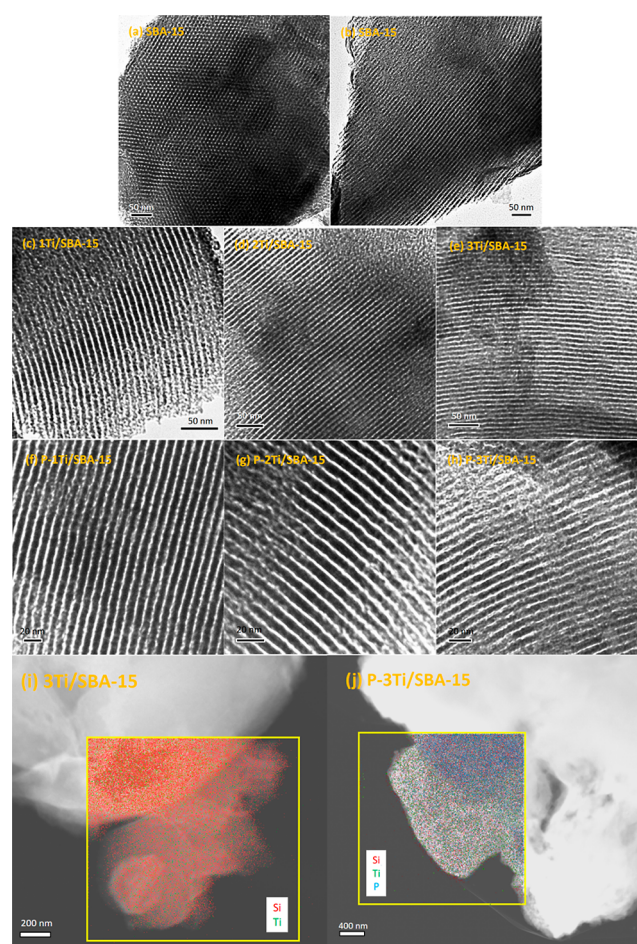

Figure 4. TEM images of (a, b) SBA-15 silica, (c) 1Ti/SBA-15, (d) 2Ti/SBA-15, (e) 3Ti/SBA-15, (f) P−1Ti/SBA-15, (g) P−2Ti/SBA-15, and (h) P−3Ti/SBA-15; STEM images and the corresponding EDX elemental mapping for (i) 3Ti/SBA-15 and (j) P−3Ti/SBA-15 (quantified elemental composition is shown in Figures S3 and S4 in the Supporting Information).

ions being 2.27 for 3Ti/SBA-15 versus 0.028 for TiO_2. Upon phosphation, the crystalline structure of PO_4^{3-}/TiO_2 remains almost unchanged (Figure S1), and the atomic ratio of tetrahedral to octahedral Ti ions increases only slightly to 0.071 (Figure 5b). For P−3Ti/SBA-15, this ratio further increases to 2.80 after phosphation transforming titania into titanium phosphate (Figure 1b). Similar peak shifting and intensity evolution were also observed for Ti $2p_{1/2}$ peak.

The total acidity and acid strength of the prepared catalysts were characterized by NH_3-TPD (Figure 6a,b and Table 2). SBA-15 silica exhibited no distinct desorption peak whereas all other samples displayed a broad peak before 400 °C (Figure 6a), which comprises three desorption peaks corresponding to acid sites of different strengths. Taking the desorption curve of 3Ti/SBA-15 and P−3Ti/SBA-15 as an example (Figure 6b): two peaks at 100−250 °C were assigned to weak acid sites, the other wide peak at 250−350 °C assigned to moderate acid sites, and no peaks of strong acid sites were found at above 400 °C. The other samples dealt with in Figure 6a gave a similar peak distribution (not shown for brevity). The weak or moderate acid strength of nTi/SBA-15 and P-nTi/SBA-15 samples infers their high activity in water, as strong LAS tend to interact with water molecule forming adducts, preventing its coordination with the reactants and leading to less amount of
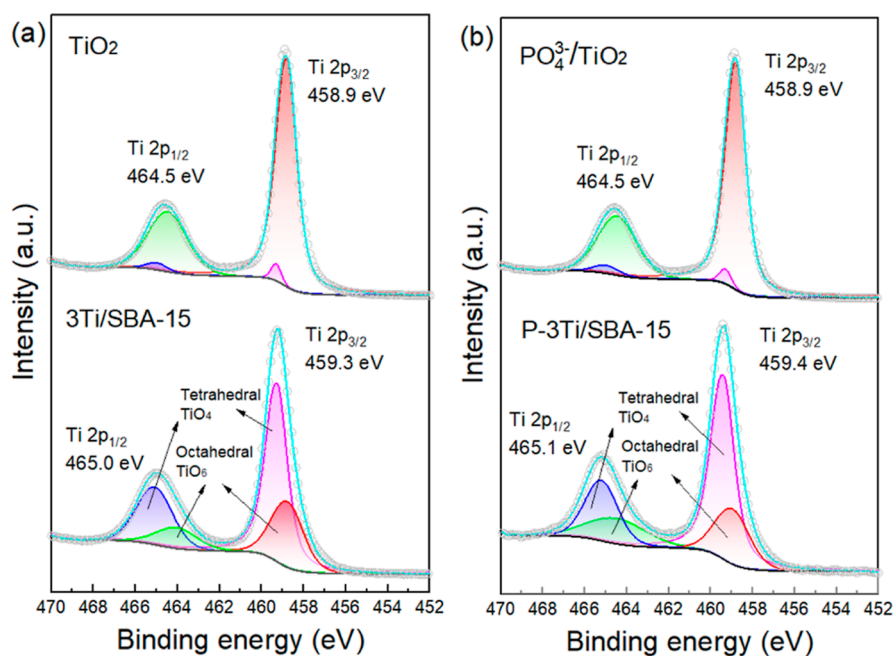
Figure 5. XPS spectra of Ti 2p on the surface of (a) anatase TiO_2 and 3Ti/SBA-15 and (b) phosphated anatase PO_4^{3-}/TiO_2 and P−3Ti/SBA-15.
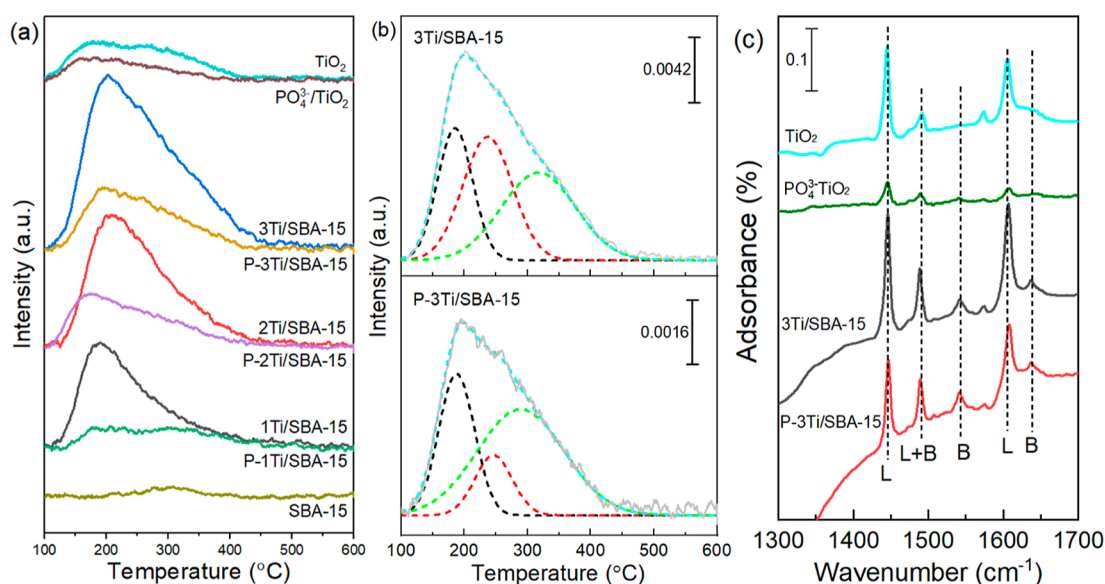
Figure 6. Characterization of the acid properties of the grafted titania and titanium phosphate on SBA-15. (a) NH_3-TPD curves of the catalyst. (b) Deconvoluted NH_3-TPD curves of 3Ti/SBA-15 and P-3Ti/SBA-15. Gray lines denote the experimental raw data; cyan dash lines denote the fitted cumulative curves; black, red, and green lines are the deconvoluted curves. (c) FTIR spectra of the adsorbed pyridine on the catalyst (with an evacuation temperature of 150 °C). LAS are denoted by L and BAS by B.

effective LAS in aqueous reaction medium.[12,41] Generally, the titania layer grafted on SBA-15 (nTi/SBA-15) affords a significantly higher acidity than bulk anatase (TiO_2), so does the corresponding titanium phosphate layer (P-nTi/SBA-15) compared with PO_4^{3-}/TiO_2. This is well consistent with (i) the by far larger portion of the unsaturated tetrahedral Ti ions (and thus the amount of LAS[12]) on nTi/SBA-15 and P-nTi/SBA-15 than that on bulk TiO_2 and PO_4^{3-}/TiO_2 (Figure 5); (ii) the much larger loading of phosphate (and thus the amount of BAS) on P-nTi/SBA-15 than PO_4^{3-}/TiO_2 (Table 1); as well as (iii) the much higher surface area of the SBA-15-supported samples (Table 1). The overall acidity of both nTi/SBA-15 and P-nTi/SBA-15 was observed to increase, despite

the decreased surface area (Table 1), with the increasing grafting cycles up to three according to NH_3-TPD results. In the catalyst preparation, the first titania grafting was mainly based on the surface Si−OH on the pristine SBA-15, while the second or third grafting cycle was based on a previous titania layer with more abundant Ti−OH groups (Scheme S1). This difference is believed to lead to a higher surface density of acid sites with more modification cycles (despite the lower surface area). Similarly, Osatiashtiani et al.[22] studied the sulfated zirconia on SBA-15 and found increased acidity and BAS/LAS ratio with the increasing layer thickness and sulfate loading. Moreover, an apparent decrease in the acidity was observed for the phosphated samples compared with TiO_2 or nTi/SBA-15

Table 2. Acidic Properties of the Grafted Titania and Titanium Phosphate on SBA-15

entry	catalyst	acidity (μmol NH$_3$/g)[a]	acidity (μmol pyridine/g)[b]		
			Brønsted	Lewis	B/L[d]
1	SBA-15	30	0	0	
2	1Ti/SBA-15	286	n.d.[c]	n.d.	n.d.
3	2Ti/SBA-15	351	n.d.	n.d.	n.d.
4	3Ti/SBA-15	503	39	117	0.33
5	P−1Ti/SBA-15	123	n.d.	n.d.	n.d.
6	P−2Ti/SBA-15	189	n.d.	n.d.	n.d.
7	P−3Ti/SBA-15	242	26	47	0.54
8	P−3Ti/SBA-15 (350 °C treated)	242	25	49	0.51
9	P−3Ti/SBA-15 (550 °C treated)	242	13	27	0.47
10	TiO$_2$	132	0	89	0
11	PO$_4^{3-}$/TiO$_2$	75	8	25	0.33

[a]Determined by NH$_3$-TPD. [b]Determined by pyridine-IR (at an evacuation temperature of 150 °C). [c]Not determined. [d]BAS to LAS molar ratio.

(Figure 6a,b and Table 2). For PO$_4^{3-}$/TiO$_2$, this is possibly because the formed Ti-O-PO(OH)$_2$ via esterification between H$_3$PO$_4$ and surface Ti−OH has covered a certain amount of LAS. For P-nTi/SBA-15, the acidity decrease might be related to the lower surface area and porosity (Table 1) and the structure re-organization causing less exposed acid sites (particularly the surface LAS) (Table 2 and Scheme S1).

Furthermore, pyridine-IR was performed to reveal the types and amounts of the acid sites on the catalyst (Figure 6c and Table 2). The adsorbances at 1540 and 1635 cm^{-1} are assigned to pyridine protonated on BAS, the adsorbances at 1446 and 1606 cm^{-1} are attributed to pyridine adsorbed on LAS, and the band at 1489 cm^{-1} is from pyridine on both LAS and BAS.[12] In line with the literature,[42,43] anatase TiO$_2$ exhibited only Lewis acidity, which decreased largely upon phosphation (PO$_4^{3-}$/TiO$_2$), together with the appearance of little amount of BAS. Comparatively, titania and titanium phosphate layers on SBA-15 exhibited a much higher amount of both LAS and BAS. Interestingly, the dispersed titania on SBA-15 also

exhibited a certain amount of BAS that is usually absent in bulk anatase TiO$_2$, which might be derived from the abundant surface Ti−OH groups. After phosphation and the formation of titanium phosphate layer, the exposed acid sites on the surface were also re-organized, leading to a decrease in the total acidity but an increase of BAS/LAS ratio, for example, from 0.33 for 3Ti/SBA-15 to 0.54 for P-3Ti/SBA-15 (Table 2). Besides this relative acid ratio, it has been elucidated that the tetrahedral Ti ions (acting as LAS) on the titanium phosphate are closely arranged with the adjacent protonated phosphate groups (behaving as BAS) in a molecular-level proximity, forming the Lewis−Brønsted acid pairs.[12] It is known from the TGA results that titanium phosphate tends to dehydrate upon thermal treatment (Figure 3). To study the effect of heat treatment on the acid properties, P-3Ti/SBA-15 samples were calcined at 350 and 550 °C for 6 h and then subjected to pyridine-IR characterization. It turned out that the acid property of the 350 °C-heated sample remained almost unchanged, while the 550 °C-heated sample exhibited a large decrease in both LAS and BAS (Table 2). Notably, because NH$_3$-TPD measurement also applied thermal treatment (up to 600 °C), the acid properties of 350 °C and 550 °C-heated samples cannot be distinguished thus giving the same acidity by NH$_3$-TPD (Table 2). The above results infer an operational temperature range below 350 °C for the P-nTi/SBA-15 catalyst when it comes to the reaction study, catalyst modification, or regeneration.

Catalytic Activity of Glucose Conversion to HMF. The typical glucose conversion network in water over Lewis and Brønsted acids is shown in Scheme 1.[12] Generally, glucose is epimerized to mannose and isomerized to fructose over the Lewis acid catalyst, and subsequently fructose is dehydrated to yield HMF, which can be further rehydrated to FA and levulinic acid over the Brønsted acid catalyst. Meanwhile, all sugars and HMF can be degraded to FA and polymerized to soluble oligomers or insoluble humins over both Lewis and Brønsted acid catalysts.[4,6,12]

The results of glucose conversion over the TiO$_2$, PO$_4^{3-}$/TiO$_2$, 3Ti/SBA-15, and P-3Ti/SBA-15 catalysts in a water-mTHF biphasic system are displayed in Figure 7. 20 wt % NaCl was added in water to promote the HMF extraction into mTHF (e.g., the partition coefficient of HMF at 150 °C

Scheme 1. Reaction Network of Glucose Conversion in Water over Lewis and Brønsted Acid Catalysts[a]
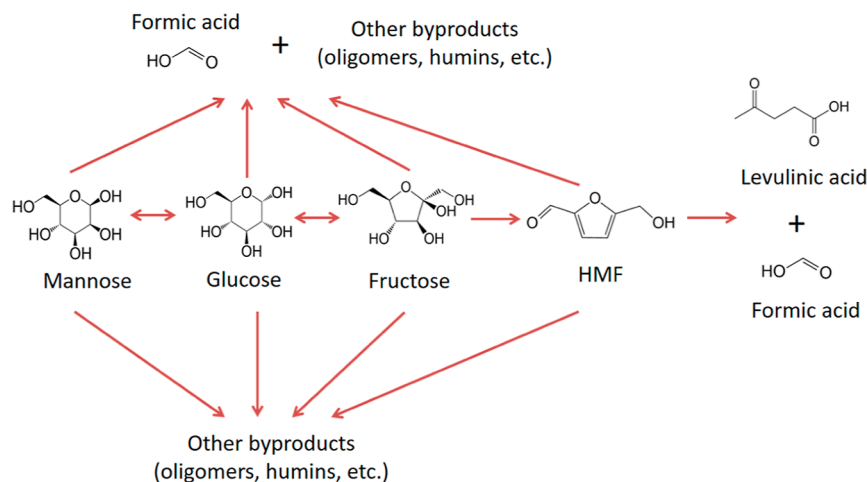
[a]Adapted from our previous work.[12]
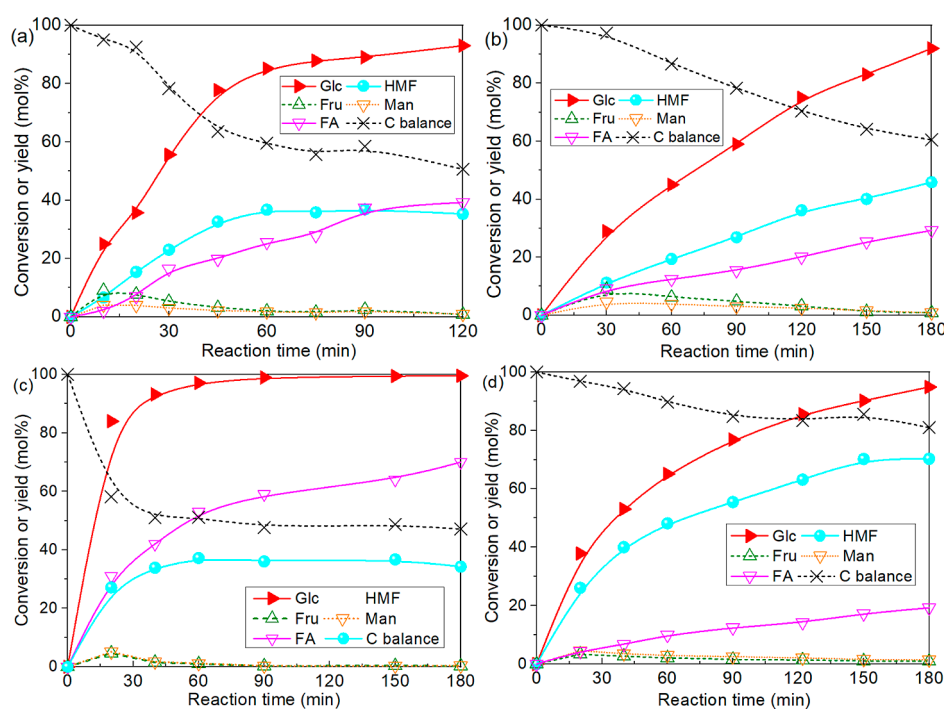
Figure 7. Glucose conversion to HMF over the prepared catalysts: (a) anatase TiO_2; (b) post-phosphated anatase (PO_4^{3-}/TiO_2); (c) 3Ti/SBA-15; and (d) P-3Ti/SBA-15. Reaction conditions: 160 °C, 0.1 M Glc, 1 mL water (containing 20 wt % NaCl) and 4 mL mTHF, weight ratio of catalyst to glucose at 1: 1. In the legend, Glc, Fru, Man, HMF, and FA denote glucose, fructose, mannose, HMF, and formic acid, respectively (the same for Figure 9).

increases from 1.01 to 2.17 after adding 20 wt % NaCl[12]). The reactions were performed at an optimized temperature of 160 °C with 0.1 M glucose (cf. more details in Figure S5 regarding the temperature optimization). As expected, mannose and fructose as the respective epimerization and isomerization products from glucose were formed at the early stages of the reaction and then prone to further chemistry such as their dehydration to HMF or degradation to FA and humins. The HMF yield increased steadily as the reaction proceeded and seemed to level off at the late stages of the reaction with a high glucose conversion over 90%, as the majority of HMF was extracted to mTHF and prevented from side reactions such as its rehydration to FA and LA and degradation to FA and humins (Scheme 1). As a result, little amount of levulinic acid (LA; < 0.5% in yield and thus not shown for brevity) was observed during the reaction in the biphasic system. Comparatively, a significantly higher amount of FA with respect to LA was formed from the degradation of sugars together with the humin formation as reflected on the evolution of carbon balance. That is, the carbon balance first decreased gradually and tended to level off at the late stage of the reaction, consistent with the stable HMF yield thereof.

In the presence of bulk TiO_2, the maximum HMF yield is ca. 36% at a glucose conversion over 90% and reaction time of 90 min (Figure 7a), indicating that the isolated LAS also catalyzes sugar dehydration to HMF but with a low selectivity.[12] A low carbon balance of 50% at the end of the reaction suggests a large humin formation, together with the formation of FA at a yield up to 40%. The PO_4^{3-}/TiO_2 catalyst exhibited a relatively much lower conversion rate (Figure 7b), due to the lower (Lewis) acidity than that of TiO_2 (Table 2). The maximum HMF yield was improved to 46% with a 92% glucose conversion after 180 min, together with a somewhat improved carbon balance to ca. 60% and suppressed FA yield

of 29%. Such an improved HMF selectivity is a result of an increased BAS/LAS ratio of 0.33 (Table 2), which to some extent initiated the tandem catalysis for glucose conversion via fructose to HMF. The dispersed titania on SBA-15 (3Ti/SBA-15) afforded a, by far, higher activity due to the higher (Lewis) acidity compared to bulk titania (Figure 6 and Table 2), as the glucose conversion reached 93% after 45 min (Figure 7c). However, the maximum HMF yield is rather limited, being only ca. 38% with a carbon balance below 50%, as the abundant reactive tetrahedral Ti ions (acting as the isolated LAS) on the titania layer were unselective and significantly promoted the humin formation. After phosphation, the formed titanium phosphate on the P−3Ti/SBA-15 catalyst provided a largely improved HMF yield (up to 71% with a glucose conversion of 90% in 150 min; Figure 7d). Simultaneously, the corresponding carbon balance was improved and kept above 85%, with the FA yield decreased to below 18%. The less humin formation was also observed during the reaction via the color change of the catalyst, for example, the 3Ti/SBA-15 catalyst turned brown while P−3Ti/SBA-15 remained still white after the reaction (Figure S6). The largely improved HMF yield over P−3Ti/SBA-15 is attributed to the selective tandem catalysis enabled by the synergy of LAS and BAS (with an LAS/BAS ratio of 0.54; Table 2). For comparison, the catalytic performance of P−1Ti/SBA-15 and P−2Ti/SBA-15 were also tested, as shown in Figure S7. The P−3Ti/SBA-15 catalyst afforded generally the highest glucose conversion (rate) and HMF yield, which is attributed to its highest acidity and possibly a better BAS/LAS ratio (Figure 6 and Table 2). To further understand the reaction, fructose conversion was performed under the same conditions over P−3Ti/SBA-15. A much faster conversion but lower maximum HMF yield than starting from glucose was observed (e.g., 48.1% HMF yield and 97.6% fructose conversion obtained at 60 min; Figure S8).

This is because of the more active fructose adsorbing on LAS leading to humins, besides the fructose dehydration to HMF over the adjacent BAS.[12] Comparatively, glucose is more stable toward condensation to humins over LAS and not active over BAS of weak acid strength.[12]

The HMF yields as a function of glucose conversion over different catalysts are summarized in Figure 8. Generally, the
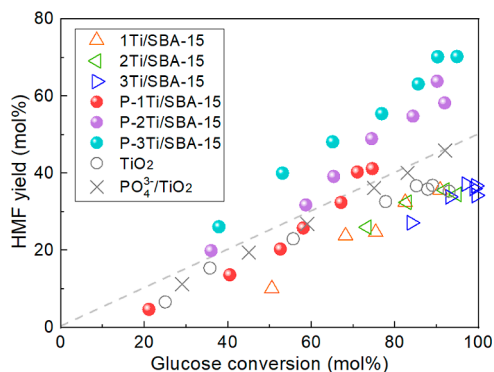

Figure 8. Relation between the HMF yield and glucose conversion over different catalysts. Reaction conditions are the same as those stated in Figure 7. The dash line represents an HMF selectivity of 50%, and symbols the experimental data.

bulk TiO₂ or dispersed titania on SBA-15 is unselective toward HMF, due to the dominant degradation reactions from sugars/HMF to FA and humins over the isolated LAS. The conventional post-phosphated titania (PO₄³⁻/TiO₂) improved the HMF selectivity only to a limited extent to ca. 50%. In comparison, the SBA-15-supported titanium phosphate gave a significantly higher HMF yield and selectivity (e.g., HMF yield of 71% and selectivity of 80% being achieved on P−3Ti/SBA-15). This is attributed to a proper cooperativity between LAS and BAS, which depends on not only the relative amount but also their close proximity on the catalyst.[12] The Lewis−Brønsted acid pairs on the titanium phosphate phase rendered a selective tandem catalysis for glucose conversion, where fructose formed from glucose and desorbed from LAS was timely dehydrated to HMF over the adjacent BAS, reducing its re-adsorption on LAS leading to humins and facilitating the liberation of LAS for another glucose turnover.[12] In summary, isolated LAS would promote the unselective humin formation.

A relatively higher BAS/LAS ratio, combined with the close proximity between LAS and BAS (realized by phosphation forming titanium phosphate), benefits the HMF synthesis. The correlation of acidity, catalytic performance, and surface P/Ti ratio of the catalysts in this work has been summarized in Figure S9 and discussed in detail in the Supporting Information.

The E-factor (kg waste per kg product) of the current catalytic process was estimated to be ca. 0.38 (based on an optimized HMF yield of 71% at a glucose conversion of 90% over the P−3Ti/SBA-15 catalyst; Figure 7d). This value is much smaller than the common level in the chemical industry (e.g., <1−5 for bulk chemicals, 5−50 for fine chemicals, and 25−>100 for pharmaceuticals),[44] indicating the more desirable sustainability of the process. Despite this, still ca. 20−30% of carbon was lost to FA or humins at this optimized HMF yield (Scheme 1). Considering that the overall BAS/LAS ratios for titanium phosphate (e.g. 0.54 for P-3Ti/SBA-15) are some-what lower than 1 (Table 2), there could be still the presence of isolated LAS on the catalyst promoting side reactions. The reason for this phenomenon could be that the hydroxyl groups of some phosphate units are too weak to act as the BAS, rendering the adjacent tetrahedral Ti ions to be an isolated LAS. Because the BAS/LAS ratio is dependent on the composition and nature of the titanium phosphate phase, an improved phosphation method could be considered in the future to further adjust the composition of titanium phosphate (i.e., further optimize the BAS/LAS ratio) to improve the process efficiency and sustainability.

Hydrothermal Stability and Reusability. The reaction of glucose conversion in aqueous media at elevated temperatures requires catalysts with a high water tolerance, including the activity of LAS in water as well as the catalyst hydrothermal stability against the leaching and collapse of porosity. The glucose conversion under heterogeneous catalysis is usually operated between 120 and 180 °C, a temperature range wherein ordered mesoporous silica tends to collapse due to the hydrolysis of Si−O−Si in water.[22,45] Since bulk TiO₂ is hydrothermally stable, the dispersion of titania as a surface layer might protect the SBA-15 support and improve its stability in the hydrothermal environment. The low angle patterns of SBA-15, 3Ti/SBA-15 and P-3Ti/SBA-15 before and after a heating treatment in water (i.e., using 0.1 g catalyst sample in 2 mL water at 160 °C for 2 h) are given in Figure 9a.
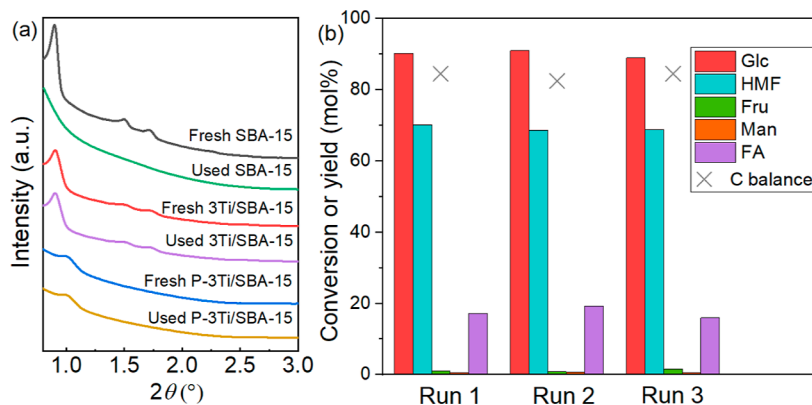
Figure 9. (a) Low-angle XRD of the fresh and hydrothermally treated (at 160 °C for 2 h) materials and (b) reusability results of the P-3Ti/SBA-15 catalyst. Reaction conditions in (b): 160 °C, 150 min, 0.1 M Glc, 20 wt % NaCl, 1 mL water, and 4 mL mTHF, weight ratio of catalyst to glucose at 1:1.

SBA-15 underwent a pore collapse upon the hydrothermal treatment, as reflected in the loss of the low angle diffraction features. In comparison, the mesoporous orderliness of 3Ti/SBA-15 and P−3Ti/SBA-15 was largely maintained, which supports our hypothesis above and is also consistent with the literature results for example, on the zirconia-grafted SBA-15.[22]

The reusability of the P-3Ti/SBA-15 catalyst was tested by running three consecutive reactions under the optimized conditions (160 °C and 150 min; Figure 9b), where the used catalyst after each run was recycled via filtration and regenerated by calcination in air at 300 °C for 6 h to remove the possibly deposited humins. Notably, such a regeneration temperature should be proper and did not alter the acid property of the catalyst, as revealed by pyridine-IR results showing unchanged acid properties of the catalyst upon a heating temperature up to 350 °C (Table 2). As shown in Figure 9b, the glucose conversion and yields of HMF and other products remain similar for all runs, indicating a good stability and reusability of the P-3Ti/SBA-15 catalyst. This is also supported by the characterization of the 1st-used/regenerated P-3Ti/SBA-15 catalyst which gave a similar surface area and acidity compared with the fresh one (Figure S10 and Table S1). ICP-AES analysis of the aqueous product solution after each run indicates that no Si was detected for all runs and P was only detected for the first two runs (128 and 67 mg/kg, respectively). The tiny amount of P leaching in the first two runs could be due to the hydrolysis of the weakly anchored phosphates on the catalyst surface, while the remaining phosphates were strongly incorporated into the framework of titanium phosphate and much more stable towards hydrolytic leaching,[12] in line with the literature findings using bulk titanium phosphate as a catalyst for glucose conversion under hydrothermal conditions.[29,46]

CONCLUSIONS

The grafting of titania on SBA-15 silica followed by its phosphation was presented to prepare a Lewis−Brønsted bifunctional solid acid catalyst for the conversion of glucose to HMF. Titania was first dispersed on SBA-15 via the surface sol−gel reaction and subsequently transformed upon phosphation into titanium phosphate with a chemical formula identified as $Ti_2O_3(H_2PO_4)_2 \cdot 2H_2O$. The ordered mesoporous structure and desirable textural properties were well maintained after the surface modifications. The dispersed amorphous titania layer on SBA-15 possessed a significantly larger portion of Ti ions in unsaturated tetrahedral coordination acting as LAS (e.g., 69.4% for 3Ti/SBA-15), compared with only 2.7% on bulk anatase titania. This rendered a more reactive nature of the dispersed titania layer which enabled its transformation into titanium phosphate upon phosphation. In contrast, the robust crystalline structure of bulk anatase TiO_2 remained unchanged after the same phosphation procedure. Therefore, nTi/SBA-15 and P-nTi/SBA-15 afford a far higher acidity than TiO_2 and PO_4^{3-}/TiO_2. The formation of titanium phosphate enabled a higher incorporation of phosphates (behaving as BAS), leading to a higher BAS/LAS ratio than that for the conventional post-phosphated bulk titania (e.g., 0.54 for P-3Ti/SBA-15 vs 0.33 for PO_4^{3-}/TiO_2). This higher BAS/LAS ratio benefited the glucose conversion to HMF, as the isolated LAS tend to promote side reactions leading to FA and humins in the short of BAS. Above that, the tetrahedral Ti ions (LAS) on titanium phosphate were closely arranged with the protonated

phosphate groups (BAS) in a molecular-level proximity and thus Lewis−Brønsted acid pairs could be formed, which enhanced the selective tandem catalysis for glucose conversion to HMF (i.e., fructose formed from glucose and desorbed from LAS was timely dehydrated to HMF over the adjacent BAS, reducing its re-adsorption on LAS leading to humins and facilitating the liberation of LAS for another glucose turnover).[12] Over the P−3Ti/SBA-15 catalyst, an optimized HMF yield of 71% was achieved from 0.1 M glucose at 160 °C after 150 min in a water(20 wt % NaCl)-mTHF biphasic system, which is significantly higher than 46% obtained over the PO_4^{3-}/TiO_2 catalyst. The SBA-15-supported titania or titanium phosphate catalysts (e.g., 3Ti/SBA-15 or P-3Ti/SBA-15) exhibited good hydrothermal stability. This stability is supported by the well-maintained ordered mesoporosity after the hydrothermal treatment at 160 °C, and the presence of no or limited leaching of Si or P during the reaction, as well as the good catalyst reusability without distinct performance loss over three consecutive reaction runs.

Generally, the dispersion of titania on SBA-15 followed by its phosphation and transformation into titanium phosphate as demonstrated in this work, represents a promising approach to synthesize bifunctional solid acid catalysts with high mesoporosity, ease of modification or transformation, and good hydrothermal stability. This benefits the use of water as a green and cheap solvent for the HMF synthesis from C6 sugars as well as other aqueous-phase reactions (involving bulky molecules) in a more sustainable way.

ASSOCIATED CONTENT

Ⓢ Supporting Information

The Supporting Information is available free of charge at https://pubs.acs.org/doi/10.1021/acssuschemeng.2c01394.

> Experimental details (material; catalyst synthesis and characterization; glucose conversion; product analysis; and calculations); wide XRD patterns of bulk TiO_2 and PO_4^{3-}/TiO_2; N_2 adsorption−desorption isotherms and pore size distributions of SBA-15, nTi/SBA-15 and P-nTi/SBA-15 catalysts; TEM/STEM images, EDX elemental mapping, and quantified elemental composition of 3Ti/SBA-15 and P-3Ti/SBA-15; glucose conversion over P-3Ti/SBA-15 at different temperatures; images of the biphasic reaction systems before and after reaction; glucose conversion over P-1Ti/SBA-15 and P-2Ti/SBA-15; fructose conversion over P-3Ti/SBA-15; correlation of the acidity and maximum HMF yield with the surface P/Ti molar ratio for different catalysts; and pore size distribution, NH_3-TPD curves, porosity and acid properties of fresh and first-used/regenerated P-3Ti/SBA-15 catalysts (PDF)

AUTHOR INFORMATION

Corresponding Author

Jun Yue − *Department of Chemical Engineering, Engineering and Technology Institute Groningen, University of Groningen, Groningen 9747 AG, The Netherlands;* Ⓞ orcid.org/0000-0003-4043-0737; Email: Yue.Jun@rug.nl

Authors

Wenze Guo − *Department of Chemical Engineering, Engineering and Technology Institute Groningen, University of Groningen, Groningen 9747 AG, The Netherlands*

Emiel J. M. Hensen − *Department of Chemical Engineering and Chemistry, Eindhoven University of Technology, Eindhoven 5600 MB, The Netherlands;* orcid.org/0000-0002-9754-2417

Wei Qi − *Guangzhou Institute of Energy Conversion, CAS Key Laboratory of Renewable Energy, Chinese Academy of Sciences, Guangzhou 510640, China;* orcid.org/0000-0002-3000-6951

Hero J. Heeres − *Department of Chemical Engineering, Engineering and Technology Institute Groningen, University of Groningen, Groningen 9747 AG, The Netherlands;* orcid.org/0000-0002-1249-543X

Complete contact information is available at:
https://pubs.acs.org/10.1021/acssuschemeng.2c01394

Notes
The authors declare no competing financial interest.

REFERENCES

(1) Corma, A.; Iborra, S.; Velty, A. Chemical routes for the transformation of biomass into chemicals. *Chem. Rev.* **2007**, *107*, 2411−2502.

(2) Huber, G. W.; Iborra, S.; Corma, A. Synthesis of transportation fuels from biomass: chemistry, catalysts, and engineering. *Chem. Rev.* **2006**, *106*, 4044−4098.

(3) van Putten, R.-J.; van der Waal, J. C.; de Jong, E.; Rasrendra, C. B.; Heeres, H. J.; de Vries, J. G. Hydroxymethylfurfural, A Versatile Platform Chemical Made from Renewable Resources. *Chem. Rev.* **2013**, *113*, 1499−1597.

(4) Guo, W.; Zhang, Z.; Hacking, J.; Heeres, H. J.; Yue, J. Selective fructose dehydration to 5-hydroxymethylfurfural from a fructose-glucose mixture over a sulfuric acid catalyst in a biphasic system: Experimental study and kinetic modelling. *Chem. Eng. J.* **2021**, *409*, 128182.

(5) Abdilla-Santes, R. M.; Guo, W.; Bruijnincx, P. C. A.; Yue, J.; Deuss, P. J.; Heeres, H. J. High-Yield 5-Hydroxymethylfurfural Synthesis from Crude Sugar Beet Juice in a Biphasic Microreactor. *ChemSusChem* **2019**, *12*, 4304−4312.

(6) Guo, W.; Heeres, H. J.; Yue, J. Continuous synthesis of 5-hydroxymethylfurfural from glucose using a combination of AlCl3 and HCl as catalyst in a biphasic slug flow capillary microreactor. *Chem. Eng. J.* **2020**, *381*, 122754.

(7) Choudhary, V.; Mushrif, S. H.; Ho, C.; Anderko, A.; Nikolakis, V.; Marinkovic, N. S.; Frenkel, A. I.; Sandler, S. I.; Vlachos, D. G. Insights into the Interplay of Lewis and Brønsted Acid Catalysts in Glucose and Fructose Conversion to 5-(Hydroxymethyl)furfural and Levulinic Acid in Aqueous Media. *J. Am. Chem. Soc.* **2013**, *135*, 3997−4006.

(8) Deng, T.; Cui, X.; Qi, Y.; Wang, Y.; Hou, X.; Zhu, Y. Conversion of carbohydrates into 5-hydroxymethylfurfural catalyzed by ZnCl2 in water. *Chem. Commun.* **2012**, *48*, 5494−5496.

(9) Karinen, R.; Vilonen, K.; Niemelä, M. Biorefining: Heterogeneously Catalyzed Reactions of Carbohydrates for the Production of Furfural and Hydroxymethylfurfural. *ChemSusChem* **2011**, *4*, 1002−1016.

(10) Kruger, J. S.; Nikolakis, V.; Vlachos, D. G. Carbohydrate dehydration using porous catalysts. *Curr. Opin. Chem. Eng.* **2012**, *1*, 312−320.

(11) Hou, Q.; Qi, X.; Zhen, M.; Qian, H.; Nie, Y.; Bai, C.; Zhang, S.; Bai, X.; Ju, M. Biorefinery roadmap based on catalytic production and upgrading 5-hydroxymethylfurfural. *Green Chem.* **2021**, *23*, 119−231.

(12) Guo, W.; Kortenbach, T.; Qi, W.; Hensen, E.; Jan Heeres, H.; Yue, J. Selective tandem catalysis for the synthesis of 5-hydroxymethylfurfural from glucose over in-situ phosphated titania catalysts: Insights into structure, bi-functionality and performance in flow microreactors. *Appl. Catal., B* **2022**, *301*, 120800.

(13) Swift, T. D.; Nguyen, H.; Erdman, Z.; Kruger, J. S.; Nikolakis, V.; Vlachos, D. G. Tandem Lewis acid/Brønsted acid-catalyzed conversion of carbohydrates to 5-hydroxymethylfurfural using zeolite beta. *J. Catal.* **2016**, *333*, 149−161.

(14) Ordomsky, V. V.; Sushkevich, V. L.; Schouten, J. C.; van der Schaaf, J.; Nijhuis, T. A. Glucose dehydration to 5-hydroxymethylfurfural over phosphate catalysts. *J. Catal.* **2013**, *300*, 37−46.

(15) Fellows, P. J. Blanching. *Food Processing Technology: Principles and Practice*; Elsevier, 2009, pp 369−380. DOI: 10.1533/9781845696344.3.369

(16) Román-Leshkov, Y.; Chheda, J. N.; Dumesic, J. A. Phase modifiers promote efficient production of hydroxymethylfurfural from fructose. *Science* **2006**, *312*, 1933−1937.

(17) Román-Leshkov, Y.; Dumesic, J. A. Solvent Effects on Fructose Dehydration to 5-Hydroxymethylfurfural in Biphasic Systems Saturated with Inorganic Salts. *Top. Catal.* **2009**, *52*, 297−303.

(18) Saha, B.; Abu-Omar, M. M. Advances in 5-hydroxymethylfurfural production from biomass in biphasic solvents. *Green Chem.* **2014**, *16*, 24−38.

(19) Guo, W.; Bruining, H. C.; Heeres, H. J.; Yue, J. Efficient synthesis of furfural from xylose over HCl catalyst in slug flow microreactors promoted by NaCl addition. *AlChE J.* **2022**, *68*, No. e17606.

(20) Okuhara, T. Water-Tolerant Solid Acid Catalysts. *Chem. Rev.* **2002**, *102*, 3641−3666.

(21) Sádaba, I.; López Granados, M.; Riisager, A.; Taarning, E. Deactivation of solid catalysts in liquid media: the case of leaching of active sites in biomass conversion reactions. *Green Chem.* **2015**, *17*, 4133−4145.

(22) Osatiashtiani, A.; Lee, A. F.; Granollers, M.; Brown, D. R.; Olivi, L.; Morales, G.; Melero, J. A.; Wilson, K. Hydrothermally Stable, Conformal, Sulfated Zirconia Monolayer Catalysts for Glucose Conversion to 5-HMF. *ACS Catal.* **2015**, *5*, 4345−4352.

(23) Guo, W.; Lu, H.; Li, X.-K.; Cao, G.-P. Tungsten-promoted titania as solid acid for catalytic hydrolysis of waste bottle PET in supercritical CO2. *RSC Adv.* **2016**, *6*, 43171−43184.

(24) Li, X.-K.; Lu, H.; Guo, W.-Z.; Cao, G.-P.; Liu, H.-L.; Shi, Y.-H. Reaction kinetics and mechanism of catalyzed hydrolysis of waste PET using solid acid catalyst in supercritical CO2. *AlChE J.* **2015**, *61*, 200−214.

(25) Sudarsanam, P.; Li, H.; Sagar, T. V. TiO2-Based Water-Tolerant Acid Catalysis for Biomass-Based Fuels and Chemicals. *ACS Catal.* **2020**, *10*, 9555−9584.

(26) Cao, Z.; Fan, Z.; Chen, Y.; Li, M.; Shen, T.; Zhu, C.; Ying, H. Efficient preparation of 5-hydroxymethylfurfural from cellulose in a biphasic system over hafnyl phosphates. *Appl. Catal., B* **2019**, *244*, 170−177.

(27) Dutta, A.; Gupta, D.; Patra, A. K.; Saha, B.; Bhaumik, A. Synthesis of 5-Hydroxymethylfururral from Carbohydrates using Large-Pore Mesoporous Tin Phosphate. *ChemSusChem* **2014**, *7*, 925−933.

(28) Weingarten, R.; Kim, Y. T.; Tompsett, G. A.; Fernández, A.; Han, K. S.; Hagaman, E. W.; Conner, W. C.; Dumesic, J. A.; Huber, G. W. Conversion of glucose into levulinic acid with solid metal(IV) phosphate catalysts. *J. Catal.* **2013**, *304*, 123−134.

(29) Dutta, A.; Patra, A. K.; Dutta, S.; Saha, B.; Bhaumik, A. Hierarchically porous titanium phosphate nanoparticles: an efficient solid acid catalyst for microwave assisted conversion of biomass and carbohydrates into 5-hydroxymethylfurfural. *J. Mater. Chem.* **2012**, *22*, 14094−14100.

(30) Atanda, L.; Mukundan, S.; Shrotri, A.; Ma, Q.; Beltramini, J. Catalytic Conversion of Glucose to 5-Hydroxymethyl-furfural with a Phosphated TiO2Catalyst. *ChemCatChem* **2015**, *7*, 781−790.

(31) Zhang, J.; Ma, Z.; Jiao, J.; Yin, H.; Yan, W.; Hagaman, E. W.; Yu, J.; Dai, S. Layer-by-Layer Grafting of Titanium Phosphate onto Mesoporous Silica SBA-15 Surfaces: Synthesis, Characterization, and Applications. *Langmuir* **2009**, *25*, 12541−12549.

(32) Shintaku, H.; Nakajima, K.; Kitano, M.; Ichikuni, N.; Hara, M. Lewis Acid Catalysis of TiO_4 Tetrahedra on Mesoporous Silica in Water. *ACS Catal.* **2014**, *4*, 1198−1204.

(33) Ichinose, I.; Senzu, H.; Kunitake, T. A Surface Sol−Gel Process of TiO_2 and Other Metal Oxide Films with Molecular Precision. *Chem. Mater.* **1997**, *9*, 1296−1298.

(34) Bortun, A. I.; Bortun, L.; Clearfield, A.; Villa-García, M. A.; García, J. R.; Rodríguez, J. Synthesis and characterization of a novel layered titanium phosphate. *J. Mater. Res.* **1996**, *11*, 2490−2498.

(35) Takahashi, H.; Oi, T.; Hosoe, M. Characterization of semicrystalline titanium(iv) phosphates and their selectivity of cations and lithium isotopes. *J. Mater. Chem.* **2002**, *12*, 2513−2518.

(36) Kőrösi, L.; Papp, S.; Dékány, I. A Layered Titanium Phosphate Ti2O3(H2PO4)2·2H2O with Rectangular Morphology: Synthesis, Structure, and Cysteamine Intercalation. *Chem. Mater.* **2010**, *22*, 4356−4363.

(37) Thunyaratchatanon, C.; Sinsakullert, W.; Luengnaruemitchai, A.; Faungnawakij, K. 5-Hydroxymethylfurfural production from hexose sugars using adjustable acid- and base-functionalized mesoporous SBA-15 catalysts in aqueous media. *Biomass Convers. Biorefin.* **2021**, *11*, 1733−1747.

(38) Gao, X.; Wachs, I. E. Titania-silica as catalysts: molecular structural characteristics and physico-chemical properties. *Catal. Today* **1999**, *51*, 233−254.

(39) León, A.; Reuquen, P.; Garín, C.; Segura, R.; Vargas, P.; Zapata, P.; Orihuela, P. A. FTIR and Raman Characterization of TiO_2 Nanoparticles Coated with Polyethylene Glycol as Carrier for 2-Methoxyestradiol. *Appl. Sci.* **2017**, *7*, 49.

(40) Sanaeishoar, H.; Sabbaghan, M.; Mohave, F. Synthesis and characterization of micro-mesoporous MCM-41 using various ionic liquids as co-templates. *Microporous Mesoporous Mater.* **2015**, *217*, 219−224.

(41) Nakajima, K.; Noma, R.; Kitano, M.; Hara, M. Titania as an Early Transition Metal Oxide with a High Density of Lewis Acid Sites Workable in Water. *J. Phys. Chem. C* **2013**, *117*, 16028−16033.

(42) Nakajima, K.; Noma, R.; Kitano, M.; Hara, M. Selective glucose transformation by titania as a heterogeneous Lewis acid catalyst. *J. Mol. Catal. A: Chem.* **2014**, *388-389*, 100−105.

(43) Noma, R.; Nakajima, K.; Kamata, K.; Kitano, M.; Hayashi, S.; Hara, M. Formation of 5-(Hydroxymethyl)furfural by Stepwise Dehydration over TiO2 with Water-Tolerant Lewis Acid Sites. *J. Phys. Chem. C* **2015**, *119*, 17117−17125.

(44) Sheldon, R. A. The E factor 25 years on: the rise of green chemistry and sustainability. *Green Chem.* **2017**, *19*, 18−43.

(45) Zhao, D.; Feng, J.; Huo, Q.; Melosh, N.; Fredrickson, G. H.; Chmelka, B. F.; Stucky, G. D. Triblock Copolymer Syntheses of Mesoporous Silica with Periodic 50 to 300 Angstrom Pores. *Science* **1998**, *279*, 548−552.

(46) Alam, M. I.; De, S.; Singh, B.; Saha, B.; Abu-Omar, M. M. Titanium hydrogenphosphate: An efficient dual acidic catalyst for 5-hydroxymethylfurfural (HMF) production. *Appl. Catal., A* **2014**, *486*, 42−48.

▣ Recommended by ACS